Research Article

Effect of Ar/CH$_4$ Mixture Ratio on Properties of Ag/C:H Nanocomposite Prepared by DC Sputtering

E. Mohsen Soltani,[1] Z. Ghorannevis,[2] and M. Shirazi[3]

[1] *Department of Physics, North Tehran Branch, Islamic Azad University, Tehran 1667934783, Iran*
[2] *Department of Physics, Islamic Azad University, Karaj 31485313, Iran*
[3] *Plasma Physics Research Centre, Science and Research Branch, Islamic Azad University, Tehran 1477893855, Iran*

Correspondence should be addressed to Z. Ghorannevis; ghoranneviszohreh@gmail.com

Ag/C:H films were deposited by DC sputtering method on Si substrates with different Ar/CH$_4$ gas mixture ratios. Effect of Ar/CH$_4$ gas mixture ratios was investigated on optical and structural properties of Ag/C:H films by FTIR spectroscopy analysis, X-Ray diffractometry (XRD), scanning electron microscopy (SEM), and atomic force microscopy (AFM), respectively. In order to evaluate the effect of gas flow ratio on the optical and structural properties of Ag/C:H films, Ar/CH$_4$ gas ratio was changed by keeping the Ar flow rate constant while varying the CH$_4$ gas flow rate (2, 5, and 10 SCCM). From FTIR analysis it was observed that increase in the Ar/CH$_4$ gas ratio results in decreasing the sputtered Ag nanoparticles and increasing of C–H bonds. Also from XRD pattern it was found that intensity of Ag crystalline plane and average grain size decrease by adding CH$_4$ to working gas admixture. From SEM and AFM micrographs, size of the grains also became smaller on the surface of the films, which will lead to decreasing the roughness of the deposited thin films.

1. Introduction

Nanoscience has developed over the last twenty years and the need for nanotechnology will only increase as miniaturization becomes more important in areas such as computing, sensor, and biomedical applications. Advances in this field widely depend on the ability to synthesize nanoparticles of various materials, sizes, and shapes as well as to efficiently assemble them into complex architectures. Nanocomposite films consisting of metals and plasma polymers have been investigated for many years since the sixties of the last century. Nano composite thin film created by silver nanoparticles has received considerable attention due to its attractive physical and chemical properties [1]. In recent years, silver nanoparticle have been widely used by the biomedical industry, for example, in medicine to reduce infections as well as to prevent bacteria colonization on prostheses [2], catheters [3, 4], vascular grafts [5], dental materials [6], stainless steel materials [7] and implants and wound and burn dressings [8, 9]. Among three metals of Ag, Au, and

Cu that display plasmon resonance in the visible spectrum, Ag exhibits the highest efficiency of plasmon excitation [10]. Moreover, optical excitation of plasmon resonances in nanosized Ag particles is the most efficient mechanism by which light interacts with matter [11]. Silver is also the only material whose plasmon resonance can be tuned to any wavelength in the visible spectrum. Therefore, metal nanoparticles exhibit remarkable physical, chemical, and biological properties. In particular, the optical and structural properties of silver nanoparticles, which vary according to their size and shape, as well as their chemical environment, have been intensively studied. Composite films metal/hard carbon were probably prepared for the first time by Craig and Harding [12], who sputtered a post cathode of Fe/Cu with a mixture of argon/acetylene in a DC cylindrical magnetron. Also silver nanoparticles have been produced using different methods such as electrochemical method [13–15], thermal decomposition [16], laser ablation [17], microwave irradiation [18, 19] and sonochemical synthesis [20]. Recently, Vaghri et al. reported different properties of Cu/C:H and Ag/C:H

[21]. Their results showed that properties of the films depend on the volume fraction ratio of the metallic phase in a composite and on the shape and size of inclusions. Mutsukura [22] used a gradual cover of the target by reaction products to deposit Ag/C:H nanocomposite films with decreasing rate of silver sputtering. Also, Kulisch et al. [23] reported the basic properties of composite films Ag/C:H:N and compared with the Ag/C:H films. They have shown that both types of films can be prepared using plasma polymerization in a low-pressure DC discharge using either argon/n-hexane or nitrogen/n-hexane as the gas mixture with simultaneous silver sputtering by means of an unbalanced magnetron. Their results showed that the incorporation of nitrogen effectively prevents the formation of carboxylate groups on the silver inclusion surfaces during the aging in the open air. Wang et al. [24] also produced TiC(Ag)/a-C:H nano-composite coating with various Ag concentrations on Si p(1 0 0) substrates. The composition and structure of as-deposited nano-composite coatings are investigated and the friction and wear behaviors are also evaluated under the ambient, high temperature and high vacuum, respectively. Their results indicated that the introduction of Ag caused a significant reduction in the residual compressive stress without considerable decrease of the hardness and improved the adhesive strength of nano-composite coating.

Magnetron sputtering has developed rapidly over the last decade to the point where it has become established as the process of choice for the deposition of a wide range of industrially important coatings. The driving force behind this development has been the increasing demand for high-quality functional films in many diverse market sectors. In many cases, magnetron sputtered films now outperform films deposited by other physical vapor deposition (PVD) processes and can offer the same functionality and the film thickness as produced by other surface coating techniques. Consequently, magnetron sputtering now delivers a significant impact in widespread applications including hard and wear-resistant coatings, low-friction coatings, corrosion-resistant coatings, decorative coatings and coatings with specific optical or electrical properties [20]. Among the sputtering techniques, DC reactive magnetron sputtering has advantage of proper control on the chemical composition, high deposition rates and low-substrate heating during the deposition of the films. It provides films of uniform thickness on large area substrates and good control of the physical properties. The physical properties of the dc magnetron sputtered films critically depends on the sputter process parameters such as sputtering pressure, substrate temperature and substrate bias voltage apart from the sputtering power [25]. DC magnetron sputtering is one of the simple deposition techniques with low operation cost but has stable growth process and high deposition rates [26]. In the present work, we report the deposition of Ag/C:H thin films at room temperature on silicon p-type substrates using a DC magnetron Sputtering system. The films are deposited with different ratio of argon/methane, and other parameters of deposition (such as current, voltage, pressure, and time of deposition) are same for all samples. Then effect of variation of Ar/CH_4 gas ratio on the optical and structural properties of Ag/C:H

films is investigated. Degree of crystallinity and crystallite size of Ag phase of deposited thin films is investigated by XRD analysis. Surface morphology of thin films is studied by scanning electron microscopy (SEM) analysis. Also the surface topography, the distributions of grain sizes on the surface of the films, and the surface roughness of obtained samples are specially investigated by atomic force microscopy (AFM) analysis.

2. Experimental

The Ag/C:H thin films are prepared by DC sputtering. A detail of this system has been reported in [21]. The glow discharge was powered by DC power supply in regime of constant current. Typical parameters are as follows: base pressure of 10^{-5} torr, discharge current and voltage are changing from 200 to 1000 mA and from 10 V to 1200 V, respectively, and distance between the target and Si substrate is 1 cm. For plasma formation, the research grade argon gas (purity 99/99%) is used. The optimum conditions that were followed to produce Ag/C:H films had the substrate holder placed at a distance of 1 cm from the silver target with the deposition time of 120 min and the power of 12 watt; all samples in this work are deposited under these conditions. The substrates, Si (1 0 0) (P-typed), were $1 \times 1 \, cm^2$ and were cleaned by ultrasonic vibration with acetone and ethanol to remove all the contaminants from their surface. The substrate temperature was 220°C for all samples, which was monitored by a digital thermocouple inserted into the substrate holder. The samples were loaded into the chamber and were fixed at the center between the two electrodes. The chamber was evacuated to a base pressure of 4.8×10^{-2} torr. The deposition process was carried out on Si substrates from a mixture of acetylene (CH_4) and argon (Ar) with different ratios. The vacuum chamber was brought to atmospheric pressure after each experiment to exchange the samples and to clean the chamber as well as the Ag electrode after removing all the bi-products of plasma deposition process. In addition Ar was used to enhance the sputtering of the Ag target. The gases were introduced into the vacuum chamber via a gas shower system to enable homogeneous plasma conditions (direct flow to the substrates). Ar/CH_4 gas ratios were changed as follows 1 : 2, 1 : 5, and 1 : 10 (This nomenclature represents the methane (CH_4) flow: 207 mL/min and argon (Ar) flows: 103 mL/min, 41.40 mL/min, and 20 mL/min, respectively, all of them identified in Table 1), and properties of these samples were compared with a sample which was produced without introducing CH_4 to the chamber. The Ag/C:H films were deposited by DC sputtering with Ar/CH_4 mixtures employing an asymmetrical capacitive coupled deposition system. For optical measurements a FTIR (Bruker, EQUT-NOX 55 model) spectrophotometer with wavenumber range of 400–4000 cm^{-1} was employed. The structure and surface morphology of the deposited Ag thin films were studied with different characterization techniques. An X-ray diffractometer (XRD) (STOE model STADI MP, Cu K_α radiation) with a step size of 0.04 and count time of 1.0 s per step was used to investigate the crystalline structure of films.
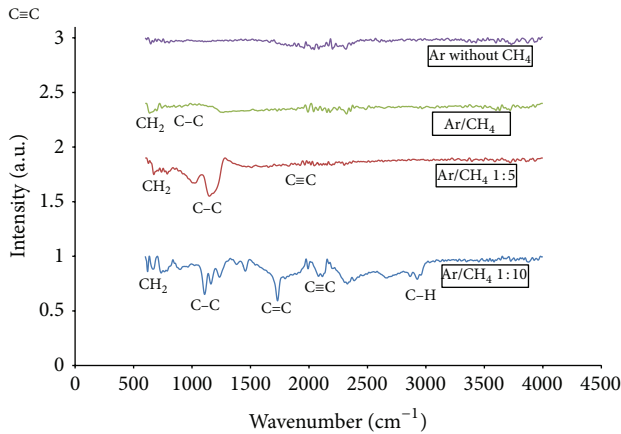
FIGURE 1: FTIR spectra of Ag/C:H thin films at different Ar/CH$_4$ gas ratios.

FIGURE 2: XRD spectra of the samples treated at different Ar/CH$_4$ gas ratios.

Also the surface morphology of thin films was analyzed by SEM (Philips XL30) and AFM (Auto Probe Pc; in contact mode, with lowstress silicon nitride tip of less than 200 Å radius and tip opening of 180).

3. Results and Discussion

3.1. FTIR Spectra Analysis. In order to evaluate the effect of gas flow on the optical and structural properties of Ag/C:H films, three samples with different ratios of gas flow (ratios of Ar/CH$_4$ was changed as 1 : 2, 1 : 5, and 1 : 10) were deposited on the silicon (100) substrate. To examine the effect of methane gas, a sample with the same conditions (power, pressure and time of the deposition) but without introducing the methane gas was prepared as a benchmark for the comparison with other samples.

Figure 1 shows the FTIR spectra of Ag/C:H thin films, which were deposited at different flow ratio of Ar/CH$_4$.

As it is shown in Figure 1, the sample, which was produced by using Ar gas, did not show the presence of bonded carbon or hydrogen peak. But with the addition of methane gas, carbon and hydrogen bonds can be seen in the FTIR spectrum. The absorption at 1650 cm^{-1} is usually assigned to the stretching of double bonds in carbon linear chains (–C=C– typical wavenumbers about 1650 cm^{-1}) and to ring vibration in aromatic hydrocarbons (typical wavenumbers near 1600 cm^{-1}). The absorption band caused by C–H stretching in various CH, CH$_2$, and CH$_3$ groups is peaked at 2912 cm^{-1}, that is, near to the wavenumber corresponding to the asymmetrical stretching in CH$_2$ (sp^3 aliphatic) group. The high-frequency tail of this band (near and above 3000 cm^{-1}) can be ascribed to stretching in various =C–H groups (both sp^2 and sp^3 configurations). The other recognized absorptions have peaks at 1460 cm^{-1} (unresolved CH$_2$ scissoring and CH$_3$ asymmetrical bending) and at 1375 cm^{-1} (CH$_3$ symmetrical bending). These witnessed a significant presence of polymeric structures (linear chains) in the films [22, 23]. On the other hand, introducing CH$_4$ to working gas mixture created these bonds, and by increase of Ar/CH$_4$ ratio polymeric bonds were increased.
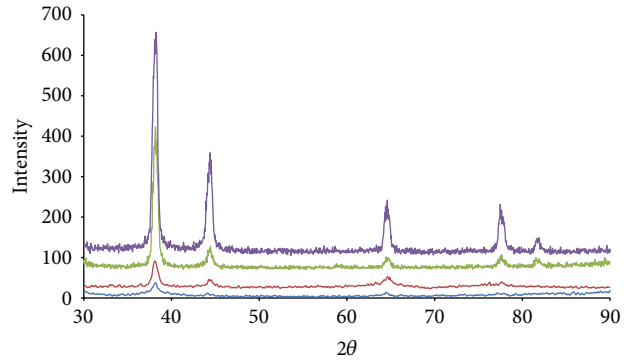
3.2. XRD Results. Figure 2 shows the XRD spectra of the samples treated with different Ar/CH$_4$ ratio in working gas mixture. From Figure 2 it is observable that the irradiated samples show the emergence of Ag crystalline phase for samples with different Ar/CH$_4$ ratios and sample, which deposited in Ar ambient. The diffraction peaks of Ag (1 1 1), Ag (2 0 0), Ag (2 2 0), and Ag (3 1 1) crystalline planes are observed at 2θ values of 38.1, 44.3, 64.9 and 77.2, respectively. The positions of the diffraction peaks are in good agreement with Joint Committee for Powder Diffraction Standards (JCPDS) standard data for Ag powders (JCPDS Card). Our observations in terms of Ag (1 1 1) and Ag (2 0 0), crystalline planes are listed in Table 1.

Note that the samples prepared without introducing methane to working gas have diffraction peaks of Ag (1 1 1), Ag (2 0 0), Ag (2 2 0) and Ag (3 1 1) crystalline planes while the deposited samples with Ar/CH$_4$ admixture gas have diffraction peaks of Ag (1 1 1), Ag (2 0 0), Ag (2 2 0) and Ag (3 1 1) crystalline planes with lower intensity. In addition to the above peaks, the diffraction peak corresponding to carbon or methane was not observed for prepared samples with Ar/CH$_4$ admixture gas. Also with increasing ratio of Ar/CH$_4$, intensity of diffraction peaks of Ag crystalline plane decreased in the XRD pattern (see Figure 2). From Figure 2 it can be observed that for the deposited samples, the intensity of the Ag diffraction peaks increases with the ratio of Ar/CH$_4$ when 2, 5 and 10 ratios were applied. The increase in relative intensity of the Ag diffraction peaks in ratio of Ar/CH$_4$ 1 : 2 can be attributed to the increase of amount of silver nanoparticles sputtered on substrate in ratio of Ar/CH$_4$ 1 : 2 which may result in the increase in diffracted photon counts if X-Ray can still penetrate up to the increased depth of silver crystalline layer. The average crystallite size is estimated using Scherer formula [21]:

$$D = \frac{0.93\lambda}{\beta \cos(2\theta)}, \tag{1}$$

where $k = 1.54$ Å is the wavelength of the source X-Ray, β is the full width at half maximum (in radians), and θ is Bragg's
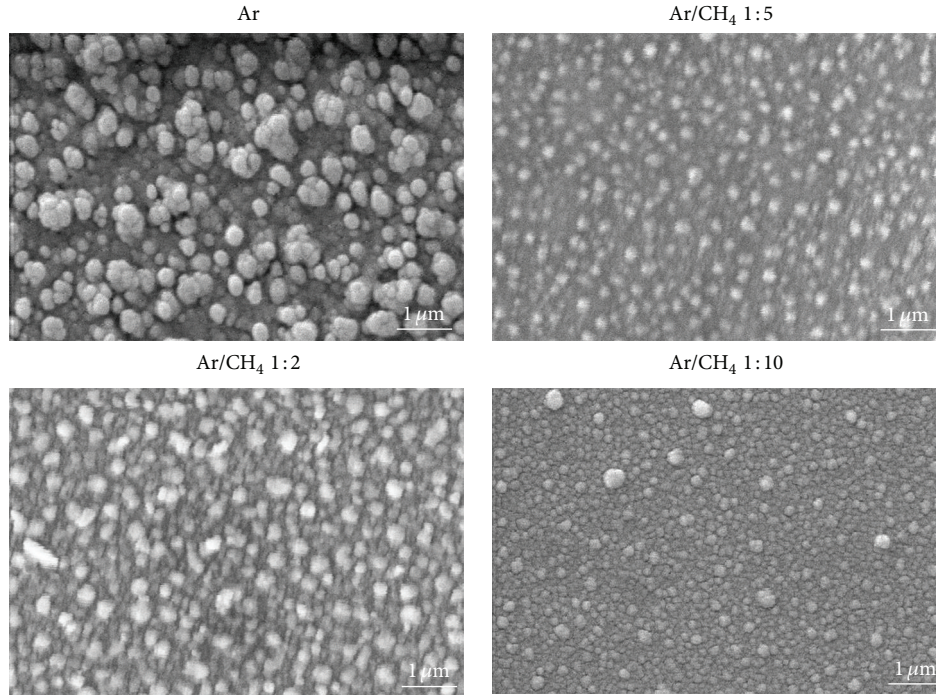
FIGURE 3: SEM micrographs of Ag/C:H films deposited at different Ar/CH$_4$ gas ratios.

TABLE 1

Sample	Ag (1 1 1)				Ag (2 0 0)			
	2θ	FWHM	Intensity	Grain size (nm)	2θ	FWHM	Intensity	Grain size (nm)
Ar	38.13	0.546	360.7	21.2	44.33	0.614	162.5	21.5
Ar/CH$_4$ 1 : 2	38.17	0.548	219.16	21.2	44.35	0.625	29.98	20.5
Ar/CH$_4$ 1 : 5	38.14	0.662	48.62	17.4	44.4	0.628	11.85	20.3
Ar/CH$_4$ 1 : 10	38.12	0.786	22.83	14.8	44.18	0.644	3.87	19.8

angle of the diffraction peak. Table 1 shows the variation of crystallite sizes of Ag (1 1 1) and Ag (2 0 0) planes for samples deposited with different Ar/CH$_4$ ratios. From Table 1 it is observable that the average crystallite size of Ag (1 1 1) and Ag (2 0 0) planes increases as the ratio of Ar/CH$_4$ decreases. This can be explained through the increase of Ag nanoparticle sputtered and decrease of C–H bonds in ratio of Ar/CH$_4$ 1 : 2.

3.3. SEM Results. Figure 3 shows the SEM micrographs of Ag/C:H thin films deposited using different ratios of Ar/CH$_4$ in working gas admixture. The SEM micrographs of the films deposited with different ratio of Ar/CH$_4$ show the crystalline growth of Ag structures by decreasing the ratio of Ar/CH$_4$ that is well in agreement with the XRD results.

Moreover it can be seen from Figure 3 that the surface morphology of the deposited thin films shows more homogeneous distribution of grains with the decreasing of the ratio of Ar/CH$_4$, which may be due to the higher ion energy flux suitable for a grain growth. Results obtained from SEM analysis reveal that the total energy deposited by the energetic ions plays the crucial role on the morphologies of the film surfaces.

3.4. AFM Results. Using AFM, the surface morphology of Ag/C:H films deposited with various ratios of Ar/CH$_4$, was analyzed. The 3D surface topography of the deposited thin films is shown in Figure 4. All the images have been obtained with a scanning area of $1\,\mu m \times 1\,\mu m$. For the case where Ag/C:H film is deposited at Ar ambient, the 3D surface topography of the deposited thin film show that the grains on the sample surfaces are the largest, and by adding CH$_4$ to working gas admixture, grains were decreased. Also as it can be seen from Figure 4, when the ratio of Ar/CH$_4$ increases from 1 : 2 to 1 : 10, a decrease in the size of most of the grains was observed. As it was previously mentioned, this may be due to a higher ion energy flux suitable for the grain growth. To analyze and compare the surface roughness of the deposited thin films, in each experiment, we measured the roughness of three random areas over the surface of the deposited thin film, and recorded the average and root mean square (rms) values of the measurements (see Table 2).
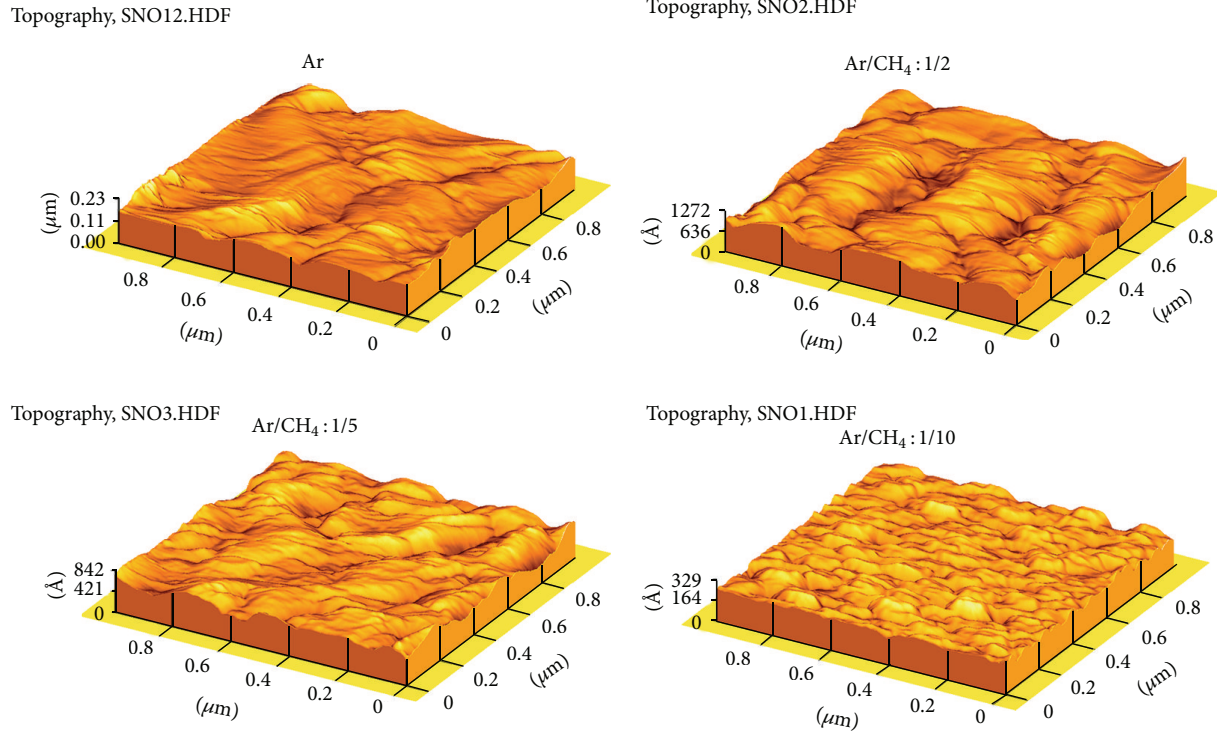
Topography, SNO12.HDF

Ar

Topography, SNO2.HDF

Ar/CH$_4$: 1/2

Topography, SNO3.HDF

Ar/CH$_4$: 1/5

Topography, SNO1.HDF

Ar/CH$_4$: 1/10

FIGURE 4: 3D surface topography AFM analysis of Ag/C:H thin films deposited at different Ar/CH$_4$ gas ratios.

TABLE 2

Sample identical	RMS roughness (nm)	Ave. roughness (nm)	Max.height (nm)	Ave. height (nm)
Ar	93	80	590	210
Ar/CH$_4$ 1 : 2	30	25	184	70
Ar/CH$_4$ 1 : 5	25	20	132	46
Ar/CH$_4$ 1 : 10	4	3	27	11

4. Conclusions

In this paper we reported the deposition of Ag/C:H thin films at room temperature on silicon p-type substrates using a DC sputtering system. In order to study the effect of the Ar/CH$_4$ flow rate on properties of Ag/C:H, the films were deposited at different ratios of Ar/CH$_4$ gas, while other experimental parameters were kept constant for all samples. Degree of crystallinity and crystallite size of Ag phase of deposited thin films were investigated by XRD analysis. Surface morphology of thin films was studied by SEM analysis. Also the surface topography, the distribution of grain sizes on the surface of the films, and the surface roughness of the samples were particularly investigated by AFM. Results of FTIR analysis showed that the introduction of CH$_4$ gas to working gas mixture created C–H stretching in various CH, CH$_2$, and CH$_3$ groups bonds, and by increasing the Ar/CH$_4$ ratio polymeric bonds were increased. In the XRD pattern the diffraction peak corresponding to carbon or methane was not observed for prepared samples with Ar/CH$_4$ admixture

gas. Intensity of diffraction peaks of Ag crystalline plane and average crystallite size of Ag (1 1 1) and Ag (2 0 0) planes increased as the ratio of Ar/CH$_4$ decreased. The SEM and AFM micrographs of the films deposited with different ratios of Ar/CH$_4$ showed the crystalline growth of Ag structures by decreasing Ar/CH$_4$ ratio, which was well in accordance with the XRD results. Also the surface morphology of the deposited thin films showed more homogeneous distribution of grains with the decrease in the ratio of Ar/CH$_4$, which might be due to the higher ion energy flux suitable for a grain growth. Furthermore, with the decrease in the ratio of Ar/CH$_4$ flow, the size of the grains became larger on the surface of the films causing increase in the roughness of the deposited thin films. Hence, with increasing the Ar flow rate from 20 to 103 mL/min, the film grain size increases from 14.8 to 21.2 nm. On the other hand, with increasing the Ar flow rate, deposition rate also increases.

References

[1] M. Urbanova, D. Pokorna, S. Bakardjieva et al., "IR laser-induced ablation of Ag in dielectric breakdown of gaseous hydrocarbons: simultaneous occurrence of metastable hcp and stable fcc Ag nanostructures in C:H shell," *Journal of Photochemistry and Photobiology A*, vol. 213, no. 2-3, pp. 114–122, 2010.

[2] M. V. Roldn, A. Frattini, O. de Sanctis, H. Troiani, and N. Pellegrini, "Characterization and applications of Ag nanoparticles in waveguides," *Applied Surface Science*, vol. 254, no. 1, pp. 281–285, 2007.

[3] H. Yin, T. Yamamoto, Y. Wada, and S. Yanagida, "Large-scale and size-controlled synthesis of silver nanoparticles under

microwave irradiation," *Materials Chemistry and Physics*, vol. 83, no. 1, pp. 66–70, 2004.

[4] Z. Zhu, L. Kai, and Y. Wang, "Synthesis and applications of hyperbranched polyesters-preparation and characterization of crystalline silver nanoparticles," *Materials Chemistry and Physics*, vol. 96, no. 2-3, pp. 447–453, 2006.

[5] A. S. Edelstein and R. C. Cammarata, *Nanomaterials: Synthesis, Properties and Applications*, Institute of Physics Publishing, Bristol, UK, 1996.

[6] M. Maillard, S. Giorgo, and M. P. Pileni, "Silver nano disks," *Advanced Materials*, vol. 14, no. 15, pp. 1084–1086, 2002.

[7] J. J. Mock, M. Barbic, D. R. Smith, D. A. Schultz, and S. Schultz, "Shape effects in plasmon resonance of individual colloidal silver nanoparticles," *Journal of Chemical Physics*, vol. 116, no. 15, pp. 6755–6759, 2002.

[8] A. R. Shahverdi, A. Fakhimi, H. R. Shahverdi, and S. Minaian, "Synthesis and effect of silver nanoparticles on the antibacterial activity of different antibiotics against *Staphylococcus aureus* and *Escherichia coli*," *Nanomedicine*, vol. 3, no. 2, pp. 168–171, 2007.

[9] S. Pal, Y. K. Tak, and J. M. Song, "Does the antibacterial activity of silver nanoparticles depend on the shape of the nanoparticle? A study of the gram-negative bacterium Escherichia coli," *Applied and Environmental Microbiology*, vol. 73, no. 6, pp. 1712–1720, 2007.

[10] U. Kreibig and M. Vollmer, *Optical Properties of Metal Clusters*, vol. 25 of *Springer Series in Materials Science*, Springer, New York, NY, USA, 1995.

[11] D. D. Evanoff Jr. and G. Chumanov, "Size-controlled synthesis of nanoparticles. 2. Measurement of extinction, scattering, and absorption cross sections," *Journal of Physical Chemistry B*, vol. 108, no. 37, pp. 13957–13962, 2004.

[12] S. Craig and G. L. Harding, "Composition, optical properties and degradation modes of Cu/(graded metal-carbon) solar selective surfaces," *Thin Solid Films*, vol. 101, no. 2, pp. 97–113, 1983.

[13] Z. Tang, S. Liu, S. Dong, and E. Wang, "Electrochemical synthesis of Ag nanoparticles on functional carbon surfaces," *Journal of Electroanalytical Chemistry*, vol. 502, no. 1-2, pp. 146–151, 2001.

[14] M. Mazur, "Electrochemically prepared silver nanoflakes and nanowires," *Electrochemistry Communications*, vol. 6, no. 4, pp. 400–403, 2004.

[15] Z. Jian, Z. Xiang, and W. Yongchang, "Electrochemical synthesis and fluorescence spectrum properties of silver nanospheres," *Microelectronic Engineering*, vol. 77, no. 1, pp. 58–62, 2005.

[16] Y. H. Kim, D. K. Lee, and Y. S. Kang, "Synthesis and characterization of Ag and Ag-SiO$_2$ nanoparticles," *Colloids and Surfaces A*, vol. 257, pp. 273–276, 2005.

[17] C. H. Bae, S. H. Nam, and S. M. Park, "Formation of silver nanoparticles by laser ablation of a silver target in NaCl solution," *Applied Surface Science*, vol. 197-198, pp. 628–634, 2002.

[18] K. Patel, S. Kapoor, D. P. Dave, and T. Mukherjee, "Synthesis of Pt, Pd, Pt/Ag and Pd/Ag nanoparticles by microwave-polyol method," *Journal of Chemical Sciences*, vol. 117, no. 4, pp. 311–315, 2005.

[19] A. Y. Vinogradov, A. S. Abramov, K. E. Orlov, and A. S. Smirnov, "Low-temperature plasma-enhanced chemical vapor deposition of hard carbon films," *Vacuum*, vol. 73, no. 1, pp. 131–135, 2004.

[20] S. M. Rossnagel, "Sputter deposition," in *Opportunities for Innovation: Advanced Surface Engineering*, W. D. Sproul and K. O. Legg, Eds., Technomic, Basel, Switzerland, 1995.

[21] E. Vaghri, Z. Khalaj, M. Ghoranneviss, and M. Borghei, "Characterization of diamond: like carbon films synthesized by dc-plasma enhanced chemical vapor deposition," *Journal of Fusion Energy*, vol. 30, no. 5, pp. 447–452, 2011.

[22] N. Mutsukura, "Photoluminescence and infra-red absorption of annealed a-CNx:H films," *Diamond and Related Materials*, vol. 10, no. 3–7, pp. 1152–1155, 2001.

[23] W. Kulisch, C. Popov, L. Zambov et al., "Investigation of the thermal stability of nitrogen-rich amorphous carbon nitride films," *Thin Solid Films*, vol. 377-378, pp. 148–155, 2000.

[24] Y. Wang, J. Wang, G. Zhang, L. Wang, and P. Yan, "Microstructure and tribology of TiC(Ag)/a-C:H nanocomposite coatings deposited by unbalanced magnetron sputtering," *Surface and Coatings Technology*, vol. 206, no. 14, pp. 3299–3308, 2012.

[25] S. V. Jagadeesh Chandra, P. Sreedhara Reddy, G. Mohan Rao, and S. Uthanna, "Growth and electrical characteristics of RF magnetron sputtered Ta$_2$O$_5$ films on Si," *Journal of Optoelectronic and Advanced Materials*, vol. 1, no. 10, pp. 496–499, 2007.

[26] P. Marwoto, "Growth of europium-doped gallium oxide (Ga$_2$O$_3$:Eu) thin films deposited by homemade DC magnetron sputtering," *Journal of Theoretical and Applied Physics*, vol. 6, pp. 17–20, 2012.